
Atomic Force Microscopy Observation of Water-Induced Morphological Changes in Y_2O_3 Monolayer Coatings

Environmental stability studies for thin-film coating materials employed on the upgraded OMEGA laser system are essential for defining acceptable air humidity levels and their control, as well as for facilitating proper thin-film coating design of long-term-use OMEGA laser optics. Moisture penetration into porous, dielectric thin-film coatings causes generally undesirable changes in the film's optical performance parameters—a fact that has been well known for some time now.^{1,2} The major effects previously observed and studied in this regard are shifts in the transmission characteristics of narrow-band filters,^{3,4} caused by the replacement of air with a 1.3-index medium inside the pores; enhanced absorption in the IR water band;⁵ and changing mechanical stress (either compressive or tensile)⁶ that renders difficult maintaining stringent wave-front-error requirements on reflective components. Thermal annealing,⁷ ion bombardment, and, more generally, preparing coatings with dense-packing structure are among the methods devised in combating water effects in dielectric films.

In addition to these macroscopic effects, certain narrow-band filters also showed microscopic morphology modifications upon water penetration. These changes took the form of circular patches that remained unaffected even by a 4-h vacuum treatment of the dielectric filter stack at 200°C.³ To our knowledge, no detailed, submicron resolution studies of such patterns were performed to date, and no fundamental insight into the growth mechanism of such patterns exists.

In this work, Y_2O_3 monolayer coatings, grown by Alpine Research Optics Inc., Boulder, CO, were used to examine AFM-resolution morphological changes caused by both a standard laboratory environment and artificial, accelerated testing in 100% relative humidity and also by droplet seeding.

Experimental Method

BK-7 glass substrates served as support for electron-beam-evaporated, 1- μ m-thick, single-layer Y_2O_3 coatings. During evaporation, substrates were held at 300°C. After shipment, samples were stored in conventional, unsealed containers. In as-received condition, the films showed no evidence of mois-

ture penetration; however, after 2-months' exposure to a fluctuating-humidity laboratory environment, reaching sporadic humidity episodes with up to 90% relative humidity, first signs of water-penetration-induced morphology changes were observed. After an additional two months, steady-state, moisture-penetration patterns developed.

Sample microscopy was carried out on a Nanoscope III (Digital Instruments, Inc.) Atomic Force Microscope using several probes, depending on sample average-surface-roughness conditions. On smooth areas with peak-to-valley variations <500 nm and lacking steep structural features, standard silicon nitride (Si_3N_4) probes proved adequate. For steep-height-gradient situations, etched silicon probes of high aspect ratio were necessary to avoid "surface-probe convolution" imaging. The Y_2O_3 surface proved to be quite stable even after hard engagement of the probe tip, and no special measures seemed necessary to prevent surface modification by the probe. A challenge did arise from the "stickiness" of the probes to water-modified sample areas, which we attributed to excessive electrostatic charging. Adjustments to the microscope feedback loop and reducing the scanning speed were successful countermeasures in this case. Microscope resolution was limited by residual system vibration noise that remained after isolation of the entire AFM/optical microscope monitor assembly on commercial vibration-isolation mounts. Cleaved-mica reference surfaces were readily imaged at atomic-scale resolution in this microscope-mounting configuration.

Artificial seeding of sample surfaces with de-ionized, distilled H_2O (18 M Ω /cm) was accomplished using a micropipette dispenser with 40-nl resolution. In the standard laboratory environment, such small water volumes evaporate from the sample surface within tens of seconds.

Moisture-Penetration Patterns

Resolving the earlier-reported, circularly symmetrical, water-penetration islands at increased resolution, one finds each island to contain a pronounced, central, pyramidal feature (occasionally split into twins or a closely packed multitude of

pyramids). Typical examples of such features are depicted in Figs. 59.1(a)–59.1(c). Their height above the adjacent film surface reaches $3\ \mu\text{m}$, and lateral extensions of up to $10\ \mu\text{m}$ have been encountered. These pyramids are surrounded by a pronounced concentric-ring pattern varying in diameter from 10 to $100\ \mu\text{m}$ [Figs. 59.2(a)–59.2(d)] and in width from 5 to $30\ \mu\text{m}$. We surmise that variations in ring sizes represent various developmental stages in ring formation.

When the features are small, i.e., at the early stages of the process, the concentric ring is not yet clearly isolated from the

central feature and contains a high density of tiny pyramids [Fig. 59.2(a)]. Upon further development, the ring separates from the central feature, leaving a concentric region with two distinct spatial and structural characteristics [Figs. 59.2(b) and 59.2(c)]. At the same time, small pyramids in the central region merge into the larger, micron-scale central pyramid [Figs. 59.1(b) and 59.1(c)].

Analyzing the region between the central pyramid and the ring, one finds the following radial subdivision: In the immediate vicinity of the central pyramid a patchwork of islands

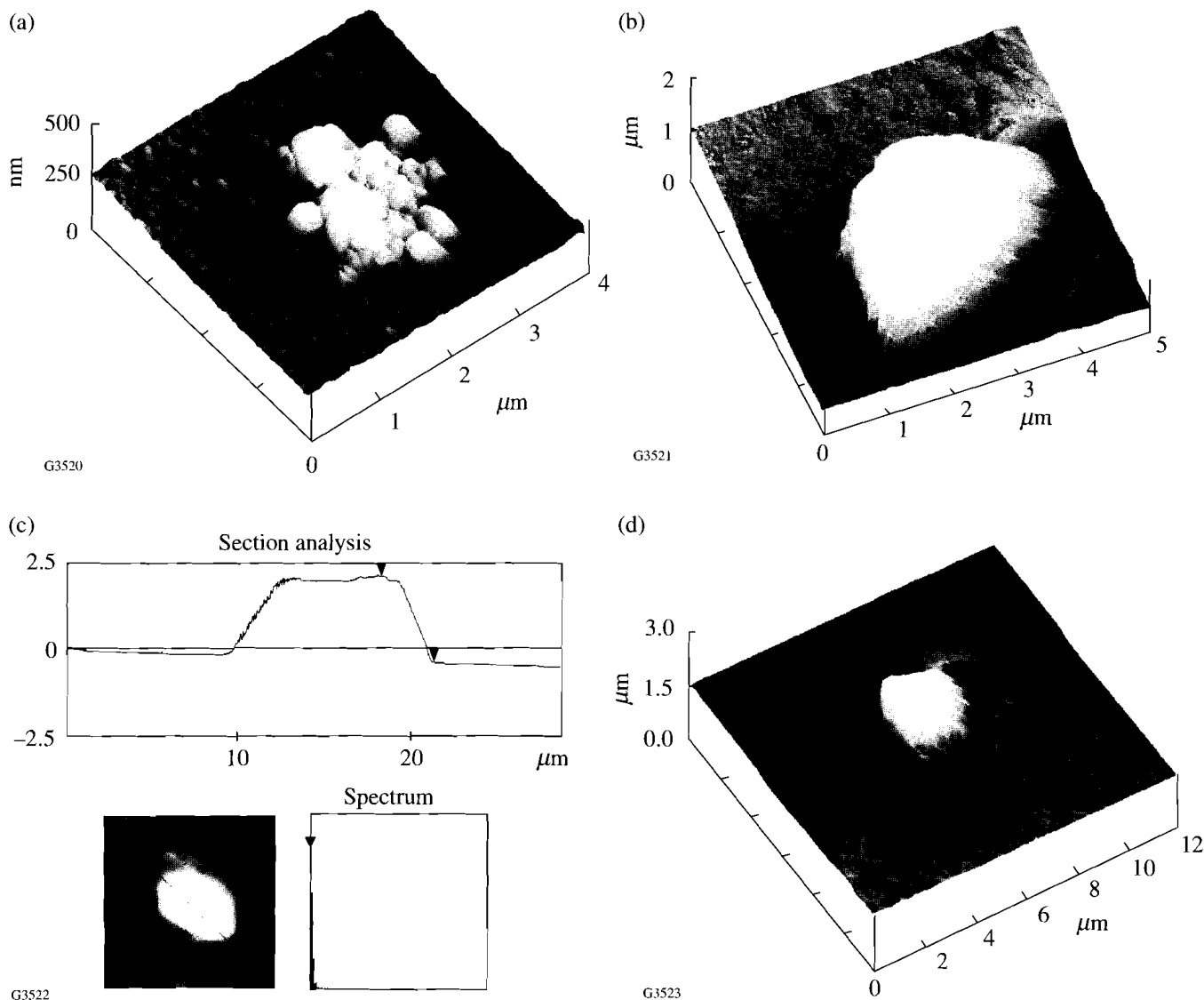


Figure 59.1

(a) Early developmental stage of a water-penetration-island central feature: small pyramids have already formed but have not yet merged. (b) Monolithic pyramidal structure with $5\text{-}\mu\text{m}$ base and $1\text{-}\mu\text{m}$ height typically found in the center of well-developed water-penetration islands. (c) Cross-sectional scan through a fully developed, $10\text{-}\mu\text{m}$ base pyramid. (d) Lower magnification view of pyramid in (b), allowing view of surrounding zone.

exists that differ from one another in both rms roughness and average height [Fig. 59.1(d)], while near the inner edge of the ring is a zone where the columnar film structure is undergoing coalescence. A similar zone of columnar coalescence is also found around the outer edge of the ring. In fact, columnar coalescence appears to be a global film process that we observed with a reduced time constant in unaffected film areas as well. At this time, the difference in rate constants between

coalescence in water-penetration island areas and coalescence in “unaffected” areas appears to be a factor of 2 to 3.

Near the central pyramid, the island topography [Fig. 59.1(d)] comprises up to 100-nm height variations among islands, with rather-smooth-surface islands always being depressed in height relative to rough-surface islands. Figure 59.3(d) shows a head-on view of the columnar structure in one of the smooth

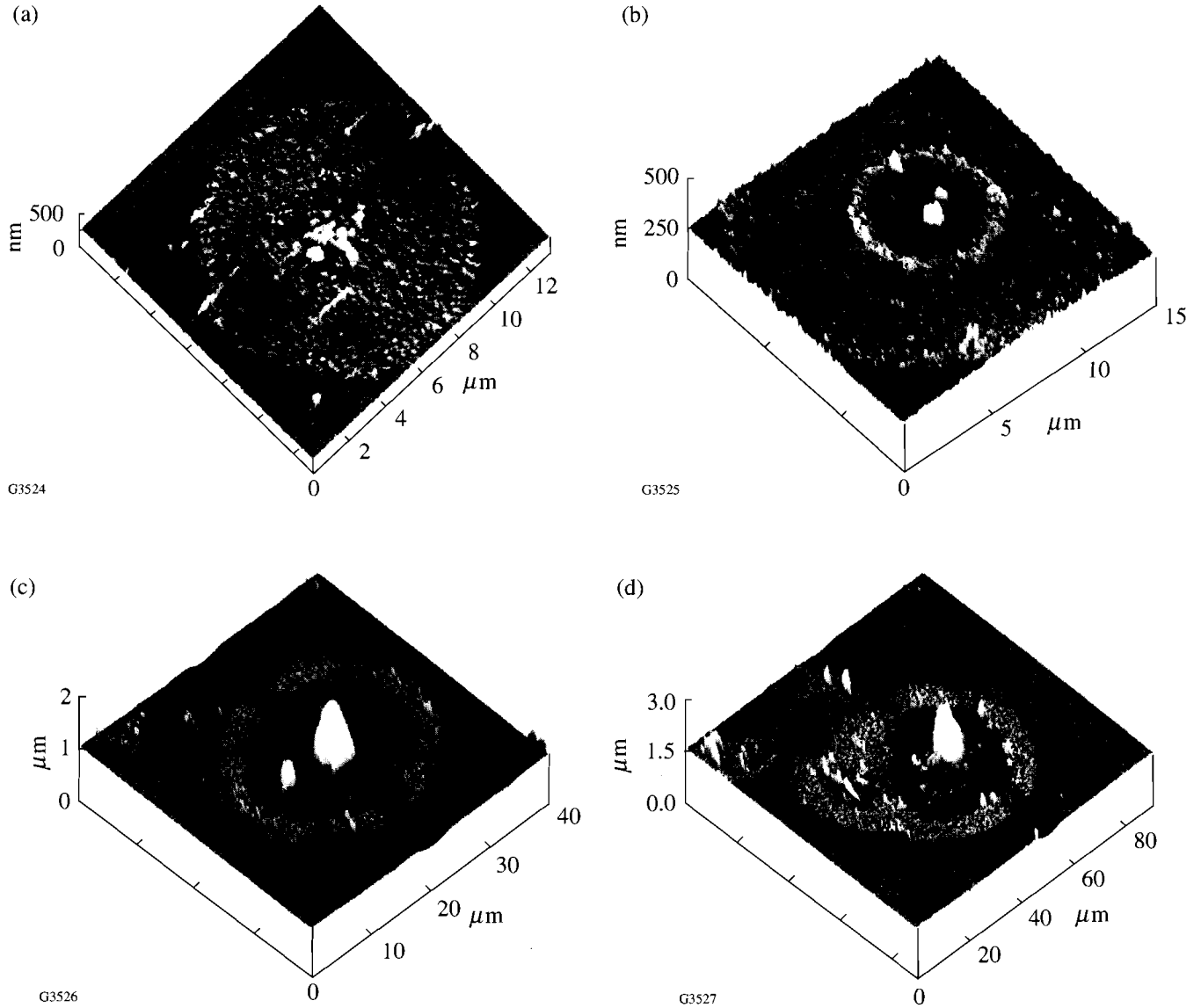


Figure 59.2

(a) View of the early stage of pattern formation: the ring (12-μm outer diameter) has not yet separated from the central feature. (b) View of ring separation in progress: the central feature is clearly developed, and a “dead-zone” between ring and central feature has evolved (18-μm ring diameter). (c) Steady-state pattern of fully developed central pyramid, ring, and intermediate zone, which contains randomly distributed, rough, and very smooth patches with height variations of up to 100 nm. (d) Very-large, >60-μm-diam, water-penetration pattern with asymmetric shape resulting from the merger of two adjacent patterns at different developmental stages.

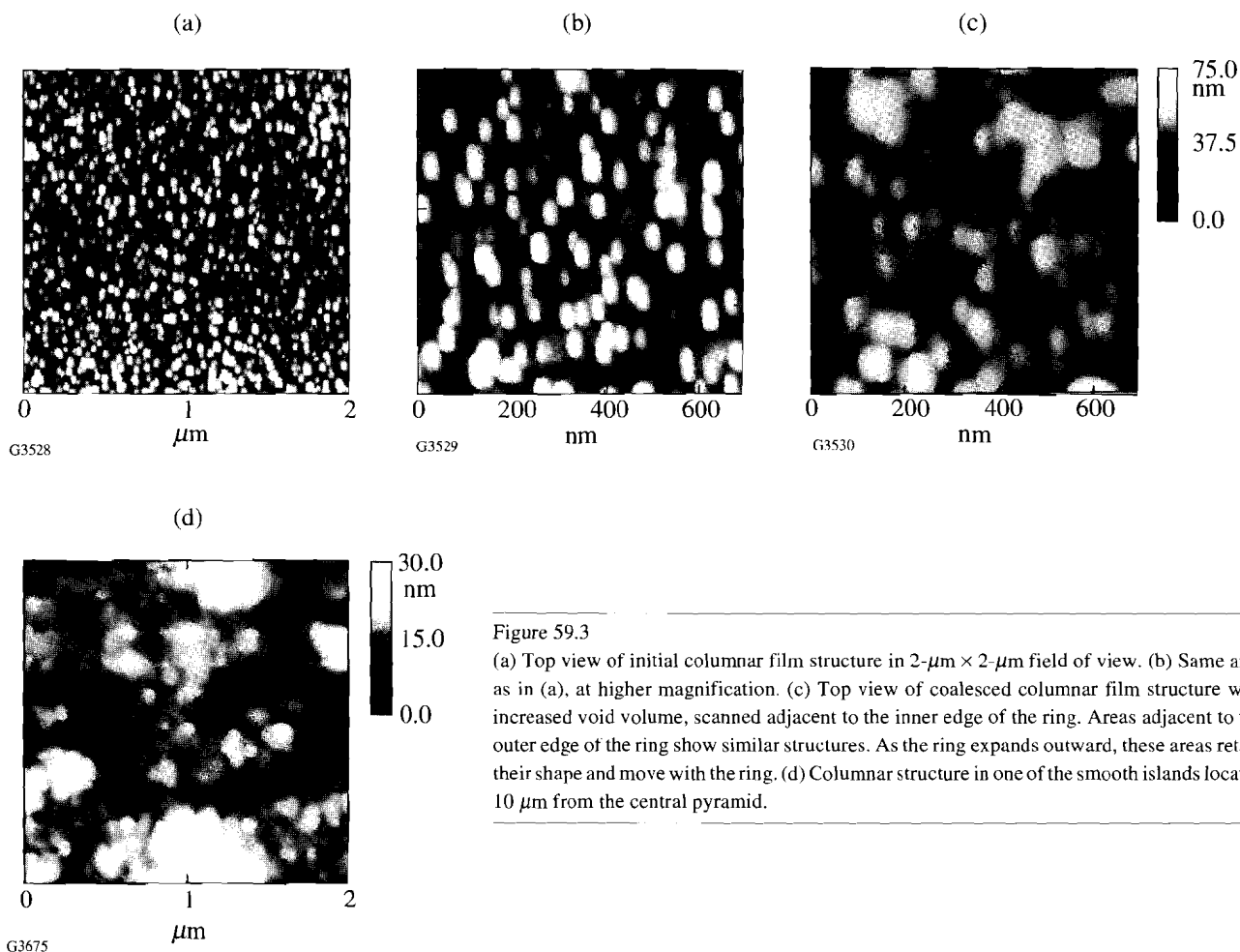


Figure 59.3
 (a) Top view of initial columnar film structure in $2\text{-}\mu\text{m} \times 2\text{-}\mu\text{m}$ field of view. (b) Same area as in (a), at higher magnification. (c) Top view of coalesced columnar film structure with increased void volume, scanned adjacent to the inner edge of the ring. Areas adjacent to the outer edge of the ring show similar structures. As the ring expands outward, these areas retain their shape and move with the ring. (d) Columnar structure in one of the smooth islands located $10\ \mu\text{m}$ from the central pyramid.

islands located $10\ \mu\text{m}$ from the central pyramid. Although columnar structure still exists, the columns' spatial frequencies have changed relative to the initial spatial frequencies shown in Fig. 59.3(a) at identical magnification and in Fig. 59.3(b) in a $700\text{-nm} \times 700\text{-nm}$ "close-up" of a film area unaffected by water (the scanned, unaffected area is $>1\ \text{mm}$ away from the center of the water-penetration island). The lower spatial frequency of the columns is accompanied by a reduction in rms roughness to below $4\ \text{nm}$.

Figure 59.3(c) depicts a $700\text{-nm} \times 700\text{-nm}$ top view of film columns and voids in the zone adjacent to the inner edge of the ring. Here, voids have widened because of columns that coalesced into coarser structures. The rms surface roughness remains unaffected by this coalescence [$8.9\ \text{nm}$ in the area of Fig. 59.3(c) versus $9\ \text{nm}$ in the initial film].

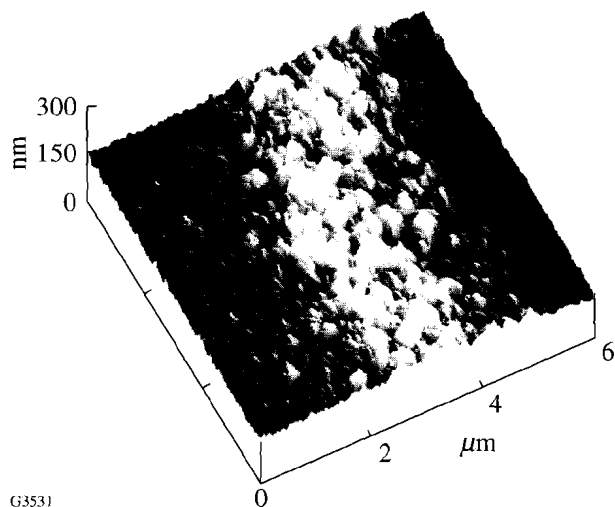
The ring itself exhibits a very rough granular structure with average grain size varying between 300 and $400\ \text{nm}$

(Fig. 59.4). The internal structure and/or porosity of these grains is yet unresolved.

The central pyramidal structures are monolithic with many, varying-size steps (1 - to 100-nm scale) decorating the surfaces (Fig. 59.5). Until now, it was not possible to unambiguously determine the crystalline structure and, by implication, the solid-state phase of the yttrium-oxide complex making up the pyramids. This critical determination was hampered by signal-to-noise limits and by probe-tip geometry restrictions. The arrival of "oxide-sharp Si_3N_4 " tips is expected to facilitate unraveling this important information that permits identifying the physico-chemical transport mechanism underlying the topographical patterns shown here.

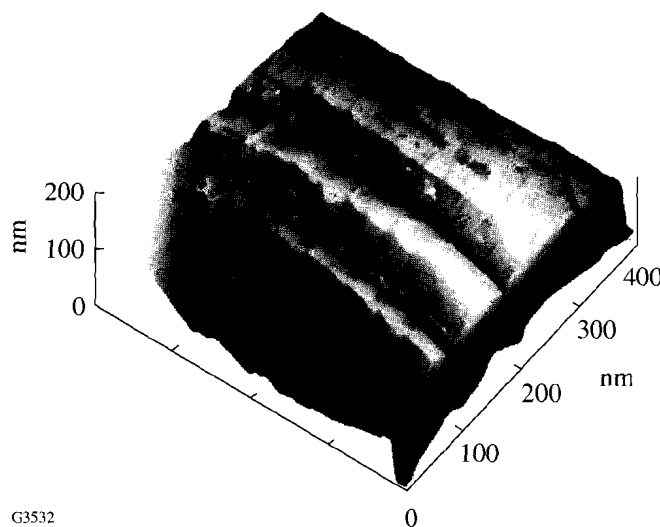
Forced-Humidity Tests

When observing moisture-penetration results from a regular laboratory environment, one needs to remain aware of contaminants in the air that potentially shift the neutral water-



G3531

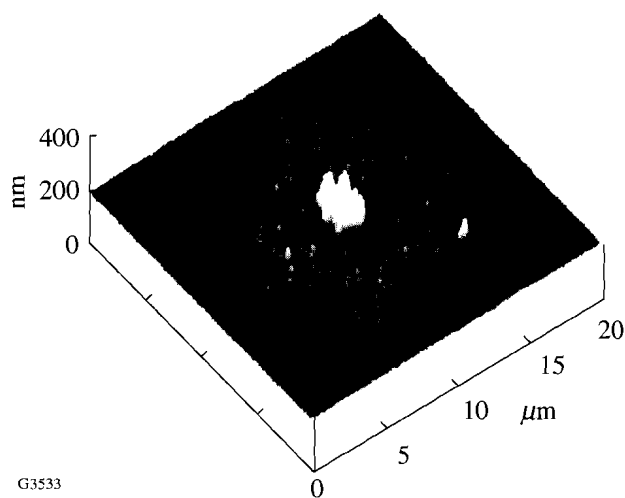
Figure 59.4
View of the 300- to 400-nm average grain size of a portion of the highly granular, well-developed ring.



G3532

Figure 59.5
View of planar dislocation steps along the trapezoidal surface of a central pyramid. The translational regularity is indicative of the pyramid's crystallinity.

vapor pH to the basic or acidic side. In order to explore to what extent pure water drives these morphological changes, an artificial, 100%-relative-humidity condition was set up, and, independently, seeding of films by microdroplets was carried out. Samples left the humidity environment only during periods of testing. After 50 cumulative hours of exposure to 100% humidity, the first, nascent water-penetration marks became observable in a form familiar to regular laboratory effects (Fig. 59.6). This proved that water alone can promote



G3533

Figure 59.6
Moisture-penetration pattern in Y_2O_3 developing under 100%-relative-humidity, 50-h exposure.

Y_2O_3 morphological changes. The question then arose as to whether forced filling of the film pores would accelerate the mass transport such that changes driven by vapor-phase concentration over periods of months could become observable within hours or minutes.

After dowsing with 300-nl droplets, which each covered 0.35 to 0.60 mm^2 , pyramidal pattern growth set in within 24 h [Figs. 59.7(a) and 59.7(b)] and continued for several weeks until an equilibrium pattern was established; however, ring structures failed to evolve. Instead, a high density of pyramids (of the order of 1 per 10 μm^2) was found, with film material between pyramids remaining [Fig. 59.7(c)] largely unmodified. Both the pattern-initiation sites and the transport mechanism for ring growth and expansion are therefore much likely different under vapor-phase conditions from mechanisms of fluid-phase chemistry active in forced seeding.

Conclusion

Long-term morphological changes induced by water penetration in Y_2O_3 monolayer films exhibit a pattern evolution that greatly influences atomic-force microscopy observations of such film surfaces. The finding that such films tend to uncontrollably change while one is watching them now has a rational basis. Growth patterns include distinct pyramidal features that either roughen the film during the early phase of growth kinetics or aggregate with time, leaving behind circular islands within which the typical dielectric-film, co-

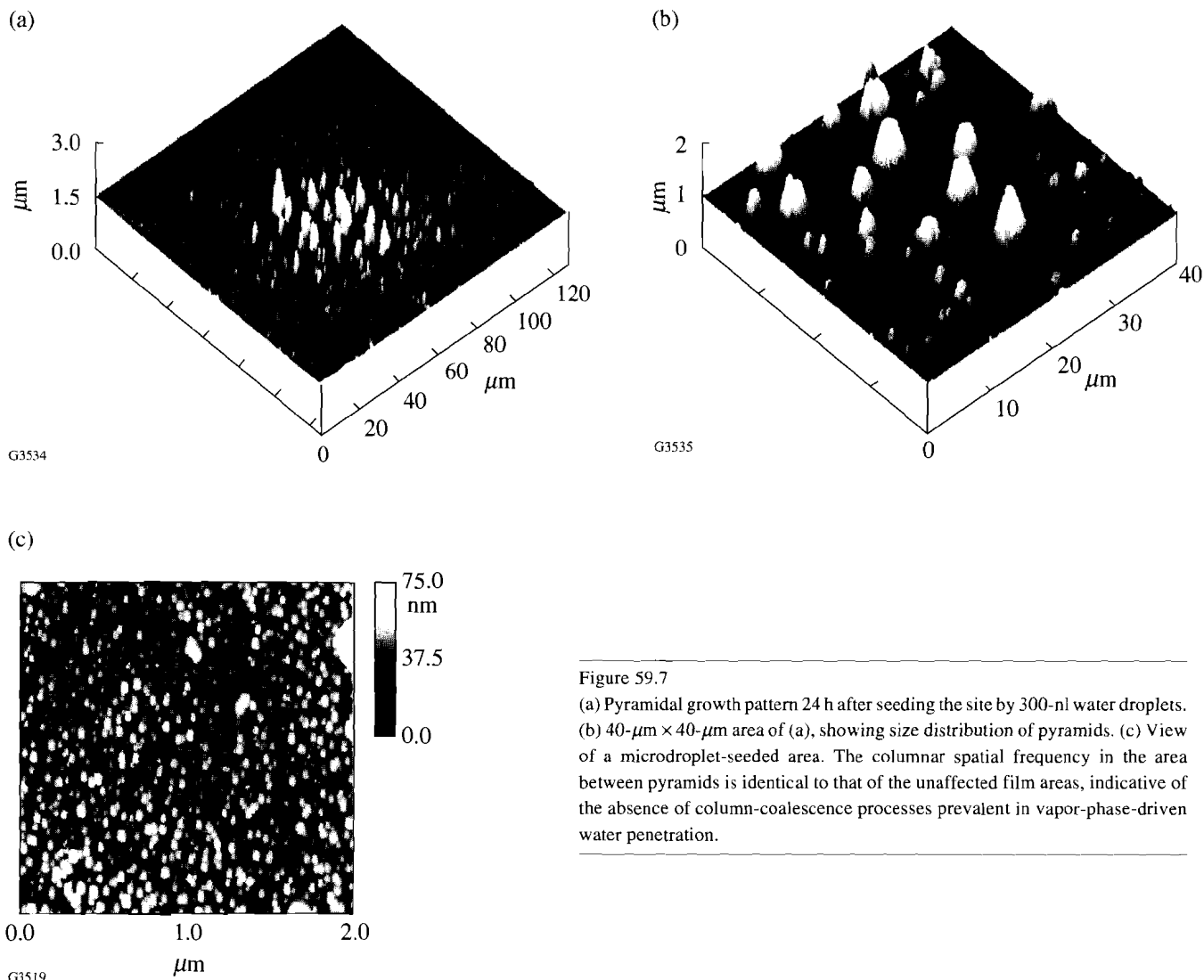


Figure 59.7
 (a) Pyramidal growth pattern 24 h after seeding the site by 300-nl water droplets.
 (b) 40- $\mu\text{m} \times 40\text{-}\mu\text{m}$ area of (a), showing size distribution of pyramids. (c) View of a microdroplet-seeded area. The columnar spatial frequency in the area between pyramids is identical to that of the unaffected film areas, indicative of the absence of column-coalescence processes prevalent in vapor-phase-driven water penetration.

luminar-growth structures have been irreversibly modified. The underlying mechanism for this redistribution of material is most intriguing but remains unresolved, pending further improvements in our experiment. It is already clear, however, that no additives to water are needed to promote the process. From an end-user concern, it is important to screen whether (and which, if any) additives, such as surfactants or solvents used in cleaning and maintenance of laser systems and infrastructures, further enhance film degradation through mechanisms evidenced here.

ACKNOWLEDGMENT

This work was supported by the U.S. Department of Energy Office of Inertial Confinement Fusion under Cooperative Agreement No. DE-FC03-92SF19460 and the University of Rochester. The support of DOE does not constitute an endorsement by DOE of the views expressed in this article. This work was carried out on equipment of the Center for Optics Manufacturing

(COM). The COM is a DOD Center of Excellence by the U.S. Army Material Command.

REFERENCES

1. H. K. Pulker and E. Jung, *Thin Solid Films* **9**, 57 (1971).
2. S. Ogura and H. A. Mcleod, *Thin Solid Films* **34**, 371 (1976).
3. H. A. Mcleod and D. Richmond, *Thin Solid Films* **37**, 163 (1976).
4. N. E. Holm and O. Christensen, *Thin Solid Films* **67**, 239 (1980).
5. T. M. Donovan and P. A. Temple, in *Laser-Induced Damage in Optical Materials: 1979* (SPIE, Bellingham, WA, 1980), Vol. 568, pp. 237-246.
6. H. Sankur and W. Gunning, *J. Appl. Phys.* **66**, 807 (1989).
7. S. G. Saxe *et al.*, *Appl. Opt.* **23**, 3633 (1984).